

Received June 1, 2016, accepted June 21, 2016, date of publication July 7, 2016, date of current version August 15, 2016.

Digital Object Identifier 10.1109/ACCESS.2016.2587581

# A New Wavelet Denoising Method for Selecting Decomposition Levels and Noise Thresholds

MADHUR SRIVASTAVA<sup>1</sup>, (Student Member, IEEE), C. LINDSAY ANDERSON<sup>2</sup>, (Member, IEEE), AND JACK H. FREED<sup>3</sup>

<sup>1</sup>National Biomedical Center for Advanced ESR Technology, Nancy E. and Peter C. Meinig School of Biomedical Engineering, Cornell University, Ithaca, NY 14853, USA

<sup>2</sup>Department of Biological and Environmental Engineering, Cornell University, Ithaca, NY 14853, USA

<sup>3</sup>National Biomedical Center for Advanced ESR Technology, Department of Chemistry and Chemical Biology, Cornell University, Ithaca, NY 14853, USA

Corresponding author: J. H. Freed (jhf3@cornell.edu)

This work was supported by the National Institute of General Medical Sciences/National Institutes of Health under Grant P41GM103521.

**ABSTRACT** A new method is presented to denoise 1-D experimental signals using wavelet transforms. Although the state-of-the-art wavelet denoising methods perform better than other denoising methods, they are not very effective for experimental signals. Unlike images and other signals, experimental signals in chemical and biophysical applications, for example, are less tolerant to signal distortion and under-denoising caused by the standard wavelet denoising methods. The new method: 1) provides a method to select the number of decomposition levels to denoise; 2) uses a new formula to calculate noise thresholds that does not require noise estimation; 3) uses separate noise thresholds for positive and negative wavelet coefficients; 4) applies denoising to the approximation component; and 5) allows the flexibility to adjust the noise thresholds. The new method is applied to continuous wave electron spin resonance spectra and it is found that it increases the signal-to-noise ratio (SNR) by more than 32 dB without distorting the signal, whereas standard denoising methods improve the SNR by less than 10 dB and with some distortion. In addition, its computation time is more than six times faster.

**INDEX TERMS** Wavelet transform, wavelet denoising, noise thresholding, noise reduction, magnetic resonance spectroscopy.

## I. INTRODUCTION

Experimental signals are often difficult to study because weak signals have a low Signal-to-Noise Ratio (SNR). Based on the discrete wavelet transform (DWT), various wavelet denoising methods like wavelet shrinkage [1]–[16], wavelet coefficient modeling [17]–[20], and wavelet transform modulus maxima (WTMM) [21]–[23] denoising methods have been developed and shown to be more effective than filtering methods [24], [25].

Although denoising increases SNR, many experimentalists are skeptical of the denoised signal as they fear inadequate noise removal and/or unknown signal distortion. More importantly, the current wavelet-based denoising methods are not very reliable in accurately retrieving the signal components, especially for weak signals that have magnitude close to noise. Also, these methods try to eliminate random noise and are not tested against systematic (or coherent) noise generated by the instrument or (e.g. biological) sample.

Another problem with current wavelet denoising methods is their practical implementation. They do not provide information regarding the choice of wavelets to use, the number of decomposition levels to denoise, nor do they have the flexibility to adjust the thresholds. A noisy signal clearly indicates its degree of uncertainty, whereas a denoised signal lacks such information. Therefore, to reduce noise, signal averaging [26] is widely used to improve experimental data. In this paper, experimental data from electron spin resonance (ESR) spectroscopy [27] is used, where signal averaging is currently the most reliable method to reduce noise. Although some signal denoising methods like filtering [28] and the traditional wavelet denoising [29] methods have been applied to ESR spectra [30], they have not yet yielded the desired results.

In this paper, a new wavelet denoising approach is presented which is based on wavelet shrinkage, that significantly improves denoising and provides clearer implementation compared to previous methods. It can be reliably used

for denoising experimental signals. The paper is organized as follows. First, a brief description of the wavelet shrinkage method is provided. Second, the issues of estimating the choice of wavelets and accurately selecting decomposition levels to denoise are discussed. Third, the new denoising method is presented. Fourth, examples of denoising using experimental results from ESR spectroscopy are presented and compared with other wavelet shrinkage denoising methods. Finally, brief comments are given on the findings and future extensions.

**II. WAVELET SHRINKAGE DENOISING METHOD**

Wavelet shrinkage methods provide effective signal denoising with minimum computational complexity. In the wavelet domain, the signal is coherent and has concentrated “energy” residing in just a few high magnitude coefficients, whereas incoherent noise is represented by a large number of coefficients with small magnitudes. This sparsity of wavelet coefficients representing the signal is exploited by wavelet shrinkage methods to separate noise from signal coefficients. Figure 1 displays a block diagram of the denoising process. Algorithm 1 summarizes the wavelet shrinkage denoising method.

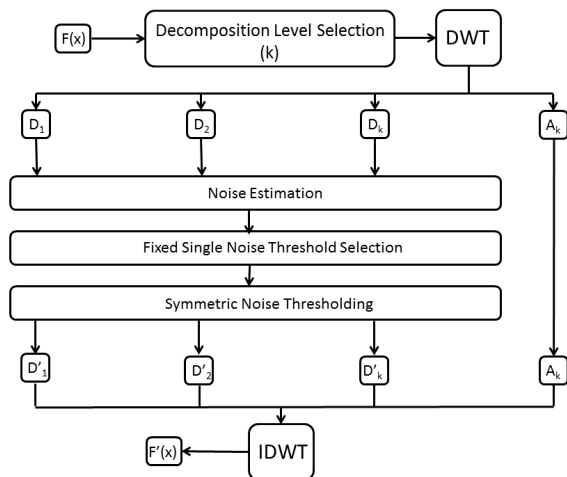


**FIGURE 1. Block Diagram of a Standard Wavelet Shrinkage Method.**

The noise threshold for the selected Detail components is obtained either using the universal threshold [31]  $\lambda = \sigma_j^{Noise} \sqrt{2 \log(N)}$ , or decomposition level dependent thresholds  $\lambda_j = \sigma_j^{Noise} \sqrt{2 \log_2 N_j}$  [32] or  $\lambda_j = \frac{\sigma_j^{Noise} \sqrt{2 \log N_j}}{\log(j+1)}$  [33], where  $N_j$  is the length of the  $j^{th}$  Detail component, and  $\sigma_j^{Noise}$  is an estimate of noise level [31]–[33]. However, state-of-the-art level-dependent noise threshold selection methods like Stein’s Unbiased Risk Estimate (SURE) threshold [34], [35] and Minmax threshold [31] are more widely used for their better performance.

Thresholding functions are then applied to remove noise using noise thresholds. Hard and soft thresholding are the most common thresholding techniques defined in

**Algorithm 1** Wavelet Shrinkage Denoising

- 1: Select a wavelet.
- 2: Select  $k$  ( $1 \leq k \leq M$ ) decomposition levels to denoise the Detail components, where  $M = \lfloor \log_2(N) \rfloor$ , and  $N = length(X)$ , and  $X$  is the discrete input signal.
- 3: Take the  $k^{th}$  level discrete wavelet transform (DWT) of the discrete input signal  $X$ , decomposing it into  $k$  decomposition levels, also referred to as  $k$  Detail components and the  $k^{th}$  Approximation component.
- 4: Estimate the noise for the  $k$  Detail components.
- 5: Calculate the noise threshold for the  $k$  Detail components.
- 6: Apply noise thresholding to the  $k$  selected Detail components.
- 7: Take the inverse discrete wavelet transform (IDWT) of the resultant  $k$  Detail components and the  $k^{th}$  Approximation component.

equations 1 and 2, respectively:

$$\tilde{w}_{j,i} = \begin{cases} w_{j,i} & : |w_{j,i}| \geq \lambda_j \\ 0 & : |w_{j,i}| < \lambda_j \end{cases} \quad (1)$$

$$\tilde{w}_{j,i} = \begin{cases} sgn(w_{j,i})(|w_{j,i}| - \lambda_j) & : |w_{j,i}| \geq \lambda_j \\ 0 & : |w_{j,i}| < \lambda_j \end{cases} \quad (2)$$

where  $w_{j,i}$  and  $\tilde{w}_{j,i}$  are noisy and denoised wavelet coefficients, respectively, at the  $j^{th}$  decomposition level and the  $i^{th}$  location of the Detail component and  $j \leq k$ . Hard thresholding is better suited when a Detail wavelet coefficient is either a signal or a noise coefficient. On the other hand, soft thresholding performs better when a Detail wavelet coefficient contains both signal and noise. There are other thresholding functions in the literature that can also be used; for example, see [9], [36]–[39].

**A. LIMITATIONS OF CURRENT SHRINKAGE METHODS**

- 1) The choice of  $k$ , the number of decomposition levels to be denoised, is arbitrary.
- 2) The choice of  $\sigma^{Noise}$  greatly influences the noise threshold  $\lambda$ , but there is no definitive way to estimate the noise value  $\sigma^{Noise}$ . Although widely used, different noise estimates yield different noise thresholds [31], [32], [35].
- 3) Assuming white gaussian noise (WGN), a single noise threshold is selected and applied to the magnitudes of both the negative and positive Detail coefficients. Other noise such as Poisson noise, Rician noise, and coherent noise are not considered for positive or negative bias in noise. Even for WGN, the assumption of no distribution bias is often flawed as will be discussed in section III.
- 4) The methods used result in fixed thresholds that are not adjusted. Flexibility in adjusting thresholds enables users to reach accurate or optimal thresholds for signals, especially when the wavelet coefficients of

weak signals are close to the maximum magnitude of noise.

Apart from the above reasons, the current denoising methods do not emphasize the choice of wavelets that is necessary to create sparsity, and separate noise and signal in the Detail components. One possible reason is that these methods are mostly applied in image processing applications which already use customized wavelets.

### III. NOISE IN WAVELET DOMAIN

It is assumed that random WGN translates into random WGN in the wavelet domain. Ideally, random white gaussian noise with zero mean should be symmetric with no overall positive and negative bias, and the magnitude of minimum and maximum values should be approximately the same. Note that the minimum is the largest magnitude among negative coefficient values ( $\max(|w_{j,i} < 0|)$ ). To test this noise behavior in the wavelet domain, simulations were run in MATLAB using the following steps:

- 1) Generate random WGN with zero mean, call it  $X$ , and length  $N$ .
- 2) Take the full scale DWT of  $X$  that results in  $\lfloor \log_2(N) \rfloor$  Detail components.
- 3) Calculate the skewness of each Detail component. The skewness is a parameter that measures positive or negative bias in a distribution with respect to the mean. For WGN (i.e. normal distribution), the skewness should be zero.
- 4) Find the magnitude of minimum and maximum value of each Detail Component.
- 5) Calculate the percentage difference between the magnitude of minimum and maximum value with respect to the minimum value between them, i.e.

$$\frac{|\max(|w_j \geq 0|) - \max(|w_j < 0|)|}{\min(\max(|w_j \geq 0|), \max(|w_j < 0|))} \times 100$$

The percentage values should be close to zero as the magnitude of minimum and maximum values would be expected to be almost the same.

The following are the simulation parameters:

- Number of Simulations: 1000-5000.
- Noise Length  $N$ : 1024-4096.
- Wavelet Families: Coiflet, Daubechises, and Symlet.

Findings:

- 1) The wavelet coefficient distribution for each Detail component has either positive or negative bias. The positive and negative bias is not correlated amongst successive Detail components.
- 2) There is a substantial difference between the magnitude of minimum and maximum values, and it increases monotonically from decomposition level 1 to  $M$ . For decomposition level 1, it is already more than 10 percent.

We believe that this behavior is due to the finite nature of discrete values and the DWT. There seems to be no correlation between the choice of wavelet and the distribution bias.

Experimental signals do not necessarily have simple WGN; their noise content is liable to be more complex and may have inherent positive or negative bias.

### IV. WAVELET BASES

It is difficult to apply the DWT without selecting an appropriate choice of wavelets. In general, standard wavelets that resemble the signal or its properties yield better signal and noise separation as well as sparsity. For example, we found that the coiflet wavelet family is better suited for cw-ESR spectra, compared to other wavelet families such as daubechies and symlets. However, a trial and error method to select the appropriate wavelet can be tedious and challenging in finding an appropriate wavelet. We recommend developing customized wavelets corresponding to the signal properties. For example, cw-ESR spectra are typically represented as blends of functions of Gaussian and Lorentzian functions [27], and hence, a specific wavelet could be designed and used for such spectra.

To effectively eliminate noise from signal coefficients, the wavelets should be designed to satisfy the following conditions:

$$\max(|w_j^{Noise} \geq 0|) < \min(|w_j^{Signal} \geq 0|) \quad (3)$$

$$\max(|w_j^{Noise} < 0|) < \min(|w_j^{Signal} < 0|) \quad (4)$$

The above conditions eliminate the need for thresholding methods (like soft-thresholding) that assume a wavelet coefficient as a sum of signal and noise coefficient, i.e.  $w_{j,i} = w_{j,i}^{Signal} + w_{j,i}^{Noise}$ . In other words, either  $w_{j,i} = w_{j,i}^{Signal}$  or  $w_{j,i} = w_{j,i}^{Noise}$ .

### V. NEW DENOISING METHOD

The new denoising method applies the wavelet shrinkage approach with the following novel features:

- 1) The decomposition levels to denoise can be determined by the user through visual inspection of the Detail and Approximation components as described below. Alternatively, an objective measure to select the  $k$  decomposition levels is provided.
- 2) Then a new noise threshold selection formula is presented that allows the user automatic adjustment of the noise thresholds. Such noise thresholds do not require the use of a noise estimation formula.
- 3) Two distinct noise thresholds are used in the thresholding function for negative and positive wavelet coefficients, respectively.
- 4) The  $k^{th}$  Approximation component is noise thresholded along with the  $k$  Detail Components.

These features are discussed below. Figure 2 illustrates the new denoising method.

#### A. DECOMPOSITION LEVEL SELECTION

Selecting decomposition levels to denoise is a major challenge to which current methods do not provide guidance.

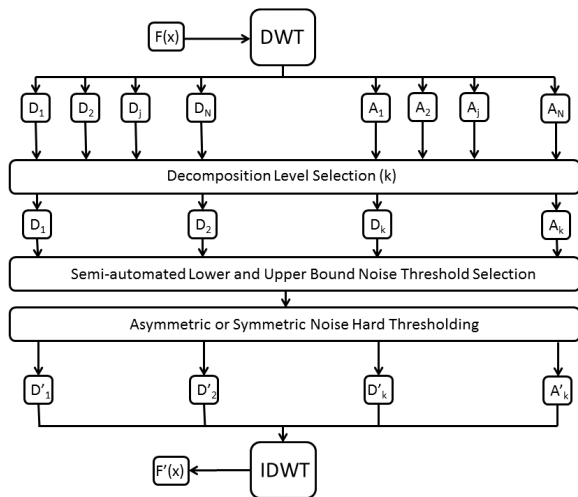


FIGURE 2. Block Diagram of the New Method.

Generally decomposition levels between 2-5 are arbitrarily selected without first examining the Detail components. A poor choice can result either in signal under-denoising or distortion, similar to that caused by poor noise thresholding. For experimental signals, this can lead to misleading analysis because the accuracy of denoising cannot be verified for every signal. A subjective and an objective method are provided to select the decomposition level  $k$ .

1) SUBJECTIVE METHOD

As all the Detail components and their corresponding Approximation components are correlated, visually observing all the components can easily allow one to select the correct decomposition level. In the new method, the user determines the Detail components to be denoised with the help of visual correlation. An easy way is to select decomposition levels until one is reached in which noise is almost indistinguishable. The location and magnitude of signal and noise in the wavelet component are also useful sources of information, especially for identifying systematic noise. In all the Detail components, signals occur in the same locations with large magnitudes, whereas random noise appears inconsistently with small magnitudes, and systematic noise usually occurs at a specific location with low magnitude. The amount of noise present in the Detail components reduces from decomposition level 1 to decomposition level  $M$  because noise usually contains more high frequencies than low frequencies. For very low SNR, initial decomposition levels like 1 and 2 may contain just noise, whereas for very high SNR, the last decomposition levels may only contain signal. Through Figure 3, decomposition level selection is illustrated by an example from ESR. Examining the figure, one can see that the Detail components at decomposition levels 1-5 contain varying amount of noise, whereas the noise (low frequency) from decomposition level 6 is extremely small and indistinguishable. The noise at and above

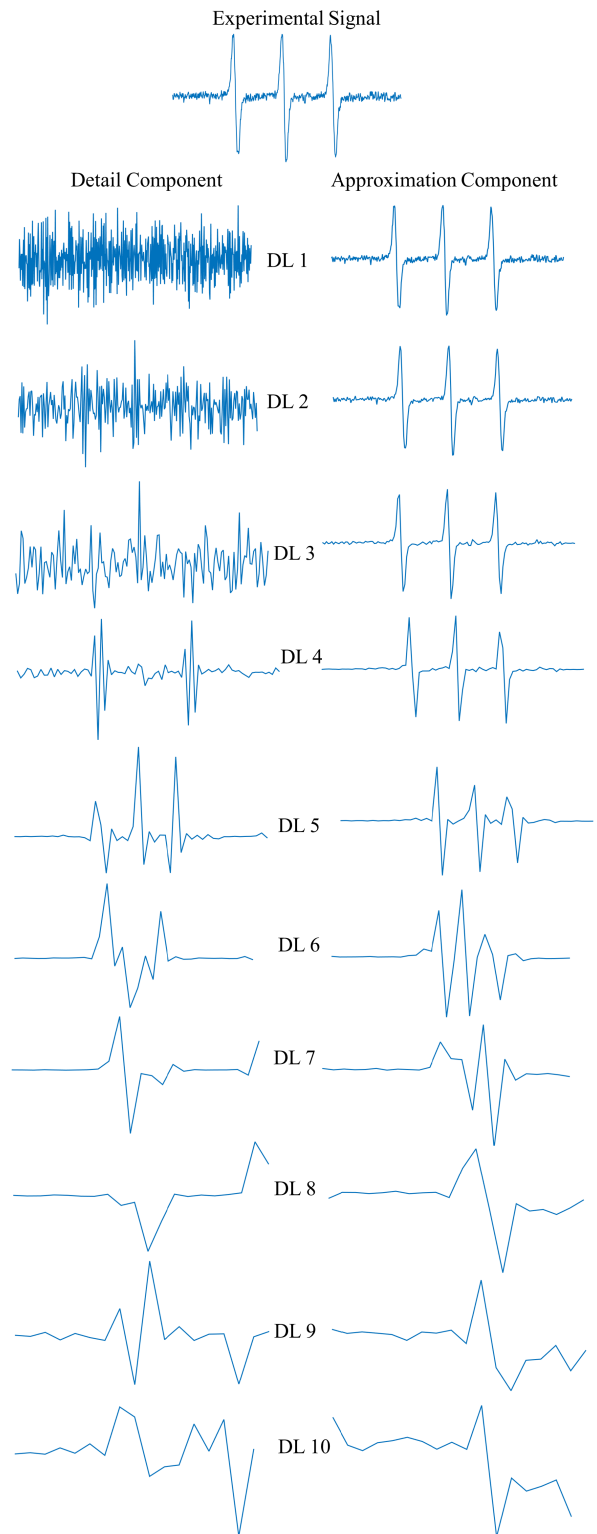


FIGURE 3. All the Detail and Approximation components of a cw-ESR spectrum. DL is the decomposition level. After examining the figure,  $k = 5$  can be confidently selected.

decomposition level 6 is represented in the Approximation component at decomposition level 5. Hence, the decomposition level  $k = 5$  can be confidently selected.

After selecting decomposition level  $k$ ,  $k$  Detail components and the  $k^{th}$  Approximation component are noise thresholded as shown in Figure 2. Coupled with noise thresholding, the decomposition level selection process also acts as a feedback for optimal thresholds and correct denoising by allowing visual comparison between the thresholded and non-thresholded wavelet components. Based on the feedback, the  $\kappa_{j,L}$  and  $\kappa_{j,H}$  values (discussed below) can be adjusted to desired thresholds. The standard state-of-the-art wavelet shrinkage methods do not exploit the correlation amongst wavelet components nor use this approach. They use non-adjustable thresholds which are optimized only for random Gaussian noise.

This subjective method is useful when a single set of experimental data needs to be denoised. It provides control to the experimentalist in selecting the decomposition levels as well as insights about the signal observed for analysis.

## 2) OBJECTIVE METHOD

The objective measure of selecting  $k$  is more appropriate for real time denoising and where extensive experimental data needs to be denoised. To obtain the decomposition levels for noise thresholding, first calculate the ‘‘peak-to-sum ratio’’ ( $S_j$ ) of the Detail components,

$$S_j = \frac{\max(|w_j|)}{\sum_{i=1}^{N_j} |w_{j,i}|} \quad (5)$$

$S_j$  reflects the sparsity of a Detail component and allows the identification of noise presence in a Detail component. A large  $S_j$  implies signal presence with only a few large coefficient values, whereas a small  $S_j$  reveals noise presence with a large number of small coefficient values.

Now the determination of the decomposition levels 1, 2, 3, . . . ,  $k$  to noise threshold is described with reference to the four categories:

- 1) Detail components that only contain noise coefficients (see DL1 in Figure 3),  $S_j \leq 0.01$ .
- 2) Detail components that mainly contain noise with very few high magnitude signal coefficients (see DL2 and DL3 in Figure 3),  $0.01 < S_j \leq 0.1$ .
- 3) Detail components dominated by signal coefficients with noise coefficients having small magnitudes (see DL4 and DL5 in Figure 3),  $0.1 < S_j \leq T_r$ .
- 4) Detail components that only contain signal coefficients, i.e. noise is no longer distinguishable (see DL6 - DL10 in Figure 3),  $S_j > T_r$ .

Here  $T_r$  is a criterion to distinguish between the Detail components of types 3 and 4 having some noise and almost no noise. Therefore,  $k = j$  where  $S_j \leq T_r$  and  $S_{j+1} > T_r$ . We find that the choice of  $T_r \approx 0.2$  leads to an effective criterion between cases 3 and 4 (More generally,  $0 \leq T_r < 1$  given that  $S_j$  of equation 5 is limited by  $0 \leq S_j < 1$ ). Note that the Detail components in the above-mentioned categories occur in sequential order (see Figure 3). Depending on the

noise level in a signal, the initial Detail component categories may or may not be present.

## B. THRESHOLD SELECTION

Wavelet shrinkage denoising depends greatly on the noise threshold value because a poor choice of threshold can result in unremoved noise or distorted signal. The presence of signal and noise coefficients in a Detail component may not result in a symmetric distribution of coefficients and zero mean. The coefficients of signal, systematic noise, and other non-symmetric noise, like Poisson noise, can create positive or negative bias in the Detail component and result in non-zero mean. Even random Gaussian noise is likely to have coefficient distribution bias due to the Detail components’ discretization and finite length as was noted in section III. In fact, it was found that symmetric Gaussian noise with zero mean has substantial differences in magnitudes of minimum and maximum noise values in the discrete wavelet domain, and the difference increases with the decomposition level (cf. section III).

Therefore, one selects two noise thresholds ( $\lambda_L$  and  $\lambda_H$ ) in the following way,

$$\lambda_{j,L} = \mu_j - \kappa_{j,L}\sigma_j \quad (6)$$

$$\lambda_{j,H} = \mu_j + \kappa_{j,H}\sigma_j \quad (7)$$

where  $\lambda_{j,L}$  and  $\lambda_{j,H}$  are the lower and upper thresholds at decomposition level  $j$ ;  $\kappa_{j,L}$  and  $\kappa_{j,H}$  are adjustable parameters for each threshold; and  $\mu_j$  and  $\sigma_j$  are the mean and standard deviation, respectively, of the wavelet component at decomposition level  $j$ , and are defined here as,

$$\mu_j \equiv \frac{\sum_{i=1}^{N_j} w_{j,i}}{N_j} \quad (8)$$

$$\sigma_j \equiv \sqrt{\frac{1}{N_j - 1} \sum_{i=1}^{N_j} (w_{j,i} - \mu_j)^2} \quad (9)$$

The two noise thresholds in equations 6 and 7 do not require the calculation of the noise level in a Detail component. They use the mean ( $\mu_j$ ) and standard deviation ( $\sigma_j$ ) of the  $j^{th}$  Detail component, which includes both signal and noise coefficients, and  $\kappa_{j,L}$  and  $\kappa_{j,H}$  are used to accurately scale  $\sigma_j$  in eliminating noise coefficients. Also, the two thresholds include the mean value  $\mu_j$ , and do not assume it to be zero.

To obtain appropriate  $\kappa$  values, we first find the minimum values of  $\kappa_{j,L}$  and  $\kappa_{j,H}$  that cover the all the coefficients in the  $j^{th}$  Detail component. Substituting minimum (peak negative value) and maximum (peak positive) values of the Detail component in equations 6 and 7, respectively, one can express them as:

$$\kappa_{j,Lmin} = \frac{\mu_j - \max(|w_j < 0|)}{\sigma_j} \quad (10)$$

$$\kappa_{j,H_{min}} = \frac{\max(|w_j > 0|) - \mu_j}{\sigma_j} \quad (11)$$

Since all the decomposition levels  $j$  ( $1 \leq j \leq k$ ) where  $S_j \leq 0.01$  (i.e., case 1) contain only noise coefficients, for these cases we can set  $\kappa_{j,L} = \kappa_{j,L_{min}}$  and  $\kappa_{j,H} = \kappa_{j,H_{min}}$ . In other words, all the coefficients of the Detail component are assigned zero.

For all the decomposition levels  $j$  ( $1 \leq j \leq k$ ) where  $0.01 < S_j < T_r$  (i.e., cases 2 and 3), both signal and noise coefficients are present. Knowing that the magnitude of a noise coefficient is less than that of the signal coefficients (cf. equations 3 and 4),  $\kappa_{j,L} < \kappa_{j,L_{min}}$  and  $\kappa_{j,H} < \kappa_{j,H_{min}}$ . One then obtains  $\kappa_{j,L}$  and  $\kappa_{j,H}$  from  $\kappa_{j,L_{min}}$  and  $\kappa_{j,H_{min}}$  using the peak positive and negative coefficient values in the following way,

$$\kappa_{j,L} = \left( \frac{S_{r,L} - S_{j,L}}{S_{r,L}} \right) \kappa_{j,L_{min}} \quad (12)$$

$$\kappa_{j,H} = \left( \frac{S_{r,H} - S_{j,H}}{S_{r,H}} \right) \kappa_{j,H_{min}} \quad (13)$$

where  $S_{r,L}$  and  $S_{r,H}$  are the reference peak-to-sum coefficient values and are defined as  $S_{r,L} \equiv \frac{S_{k,L} + S_{k+1,L}}{2}$  and  $S_{r,H} \equiv \frac{S_{k,H} + S_{k+1,H}}{2}$ .  $S_{j,L}$  and  $S_{j,H}$  are the peak-to-sum ratios of the negative and positive coefficient values, respectively. They are calculated from equation 5 as,

$$S_{j,L} = \frac{\max(|w_j < 0|)}{N_k} \sum_{i=1}^{N_k} |w_{j,i} < 0| \quad (14)$$

$$S_{j,H} = \frac{\max(|w_j \geq 0|)}{N_j} \sum_{i=1}^{N_j} |w_{j,i} \geq 0| \quad (15)$$

By separating the wavelet coefficients at a decomposition level into two groups, one having negative values and other having positive values, the number of coefficient values as well as their sum in each category is reduced. However, the peak value remains at a similar level. In other words, one expects  $\max(|w_j < 0|) \approx \max(|w_j \geq 0|)$ , and one of them

is in fact  $\max(|w_j|)$ , whereas  $\sum_{i=1}^{N_j} |w_{j,i} < 0|$  and  $\sum_{i=1}^{N_j} |w_{j,i} \geq 0|$  are both less than their sum  $\sum_{i=1}^{N_j} |w_{j,i}|$ . Thus  $S_{j,L}; S_{j,H} > S_j$ .

Instead of manually selecting the  $\kappa$  values, it is found that equations 12 and 13 accurately estimate the required  $\kappa_{j,L}$  and  $\kappa_{j,H}$  values.

The Detail components at decomposition levels  $j > k$  (i.e.,  $S_j > T_r$ ) are not noise thresholded as they contain only signal coefficients or signal and indistinguishable low frequency noise coefficients.

Although  $\kappa_{j,L}$  and  $\kappa_{j,H}$  will optimally select the noise thresholds, they may require minor adjustment by user intervention for the following three exceptions:

- 1) Even for  $S_j \geq 0.01$ , a Detail component can have only noise coefficients due to one or more large random noise spikes. In this case,  $\kappa_{j,H} = \kappa_{j,H_{min}}$  and  $\kappa_{j,L} = \kappa_{j,H_{min}}$ , instead of equation 12 and 13.
- 2) In a noise-dominated Detail component, either positive or negative coefficients are all noise, requiring readjustment  $\kappa_{j,H} = \kappa_{j,H_{min}}$  or  $\kappa_{j,L} = \kappa_{j,H_{min}}$ , respectively.
- 3) When small signal and large noise coefficient values are comparable,  $\kappa_{j,L}$  and/or  $\kappa_{j,H}$  may require a slight increase or decrease in their values to separate signal and noise coefficients.

### C. THRESHOLDING FUNCTION

This new approach to denoise the signal uses hard thresholding coupled with the above noise threshold selection method. Unlike other thresholding techniques, hard thresholding ensures that the signal wavelet coefficients are not distorted by the noise thresholds, especially when signal and noise coefficients are disjoint and not superimposed. With appropriate wavelet selection, the noise present at a signal location is separated in the initial decomposition levels and is removed using noise thresholding. Hard thresholding is now carried out in the following way,

$$\tilde{w}_{j,i} = \begin{cases} 0 & : \lambda_{j,L} \leq w_{j,i} \leq \lambda_{j,H} \\ w_{j,i} & : \text{otherwise} \end{cases} \quad (16)$$

$w_{j,i}$  is the  $i^{th}$  Detail coefficient at  $j^{th}$  decomposition level,  $\tilde{w}_{j,i}$  is the thresholded wavelet coefficient, and  $\lambda_{j,L}$  and  $\lambda_{j,H}$  are the two noise thresholds obtained from equations 6 and 7. The above equation is a generalized form of the hard thresholding function shown in equation 1. If  $\kappa_{j,L} = \kappa_{j,H}$  and  $\mu = 0$ , then  $|\lambda_{j,L}| = |\lambda_{j,H}| = \lambda_j$ , and equation 16 becomes equation 1.

### D. DENOISING THE APPROXIMATION COMPONENT

Current wavelet shrinkage methods do not denoise the Approximation component because the noise thresholding relies on sparsity of wavelet coefficients for estimating noise and selecting thresholds. Experimental signals often contain substantial low frequency noise, especially at low SNR, that impedes analysis. The Detail components that represent low frequency noise are non-sparse, restricting the effectiveness of noise thresholding. However, the Approximation component can also contain low frequency noise. Thus, it would be desirable to remove the Approximation component's low frequency noise. Depending on the signal properties and the choice of wavelet, the  $k^{th}$  Approximation component can represent low frequency noise and signal coefficients in a relatively sparse manner. The signal coefficients will have larger values than the noise coefficients. This new approach denoises the  $k^{th}$  Approximation component to eliminate low frequency noise. Similar to the Detail components, the noise thresholds for the Approximation component is selected using the Approximation coefficients in equations 6 and 7, where  $\kappa$  values are obtained from equations 12 and 13.

The thresholding function in equation 16 is then applied to remove the noise. This is shown in the block diagram of Figure 2.

## VI. ESR EXPERIMENTS AND RESULTS

### A. ESR METHODOLOGY AND SAMPLE PREPARATION

Most of the ESR experiments were performed at 20°C on a commercial spectrometer (BRUKER ELEXYS-II E500) at a standard microwave frequency of 9.4 GHz (X-band) corresponding to a dc magnetic field of 0.34 Tesla (cf. Figs. 3-8). These results are referred to as example 1. In these experiments the microwave frequency is held constant, while the magnetic field is swept through resonance to obtain the ESR spectrum [27]. The sample consisted of 4  $\mu\text{L}$  of a 100  $\mu\text{M}$  aqueous solution of the commonly used spin-probe molecule Tempol (4-Hydroxy-2,2,6,6-Tetramethylpiperidine 1-oxyl) [27], [40]–[43]. It was placed in a glass capillary of 0.8 mm ID, which was then introduced into the microwave cavity situated between the pole caps of the dc magnet. The magnetic field was then swept over a range of 60 G corresponding to the resonant spectral range which took 2 minutes, and a 82 ms time constant was used. The spectral data consisted of 4096 points along the magnetic-field sweep. In addition, small coils placed at the sides of the resonator provided a small magnetic field modulation of  $\pm 0.02$  G at a frequency of 100 kHz. The 100 kHz modulated ESR signal was detected with a lock-in detector at this frequency, providing the first derivative of the absorption signal [27], [44]. Low power (0.2 mW) microwave radiation was used to avoid saturating the ESR signal. Multi-scan experiments were performed with a delay of 4 s between scans. The results of these scans were then averaged. The ESR spectrum in Figure 3 was obtained under very similar conditions, also for the Tempol spin-probe.

In example 2, an ESR spectrum (Figure 9) was obtained under different conditions to provide a more complex spectrum for denoising. It was obtained on a home-built (ACERT) 95 GHz ESR spectrometer [43] with a dc magnetic field of 3.3 Tesla at 25°C. The sample here contained ca. 5  $\mu\text{L}$  of phospholipid vesicles doped with 0.5% of a lipid spin label: 16-PC (1-acyl-2-[16-(4,4-dimethyloxazolidine-N-oxyl)stearoyl]-sn-glycero-3-phosphocholine) in the fluid phase that had been suspended in water. It was placed in a disc-like sample holder utilized for millimeter-wave ESR methodology [43], [45]. The acquisition parameters were: sweep width of 250 G, sweep time of 2 min with a time constant of 100 ms. The millimeter-wave power was 16 mW and the spectrum consists of 512 points. The field modulation parameters were: 6 G modulation amplitude and 100 kHz modulation frequency. The spectrum in Figure 9 is the average of 100 scans. The time between scans was 3 s.

### B. EXPERIMENT

These experimental cw-ESR spectra were used to test and compare the denoising methods. By averaging different

numbers of scans, different SNRs were obtained. In the case of typical cw-ESR spectra, such as those in Figures 3-9, they have regions with zero signal, aiding in the estimation of noise. The noise in these experiments is predominantly random Gaussian noise, as is typical in ESR. Hence, the cw-ESR spectra reveal the effectiveness of denoising methods at places where the signal is present as well as absent. In Figure 4 two noisy spectra from a single sample are shown, but at different SNRs obtained by signal averaging 4 and 16 scans, respectively. As a reference, the signal averaged over 500 scans is used for comparison with the denoised signals. The SNR was calculated as,

$$SNR = \frac{Signal_{Peak-to-Peak}}{Noise_{rms}} \quad (17)$$

or in decibels (dB)

$$SNR = 20 \log_{10} \left( \frac{Signal_{Peak-to-Peak}}{Noise_{rms}} \right) \quad (18)$$

where *rms* is the root mean square. The SNR measures both distorting (i.e., structural) and non-distorting (i.e., non-structural) noise in the signal, but it cannot differentiate between them. Usually, the structural fidelity of the noisy or denoised signal with respect to a reference signal can be visually observed. Of course, the retention of signal structure is important. Apart from visually observing and comparing the noisy or denoised signal with a reference signal, an objective measure, the structure similarity index measure (SSIM) [46] was used. It enabled the estimation of the structural similarity or fidelity of the noisy and of the denoised signals at 4 and 16 scans with respect to the reference 500 scan signal. The SSIM is calculated as,

$$SSIM(X, Y) = \frac{(2\mu_X\mu_Y + c_1)(2\sigma_{XY} + c_2)}{(\mu_X^2 + \mu_Y^2 + c_1)(\sigma_X^2 + \sigma_Y^2 + c_2)} \quad (19)$$

where  $X$  is either the noisy or denoised signal;  $Y$  is the reference signal;  $\mu_X$  and  $\mu_Y$  are the mean values of  $X$  and  $Y$ , respectively;  $\sigma_X$  and  $\sigma_Y$  are the standard deviation values of  $X$  and  $Y$ , respectively;  $\sigma_{XY}$  is the covariance of  $X$  and  $Y$ ; and  $c_1$  and  $c_2$  are small positive constants used for stabilizing each term. The SSIM value ranges within  $[-1, 1]$ , and achieves 1 when  $X$  is identical to  $Y$  ( $SSIM(X, Y) = SSIM(X, X) = SSIM(Y, Y) = 1$ ). The more that  $X$  structurally resembles  $Y$ , the SSIM value will be closer to 1. MATLAB was used to calculate the SSIM.

An ESR spectrum is frequently composed of Lorentzian and Gaussian functions, or mixtures of both. The examples of Figures 3-8 are simple Lorentzians, whereas that of Figure 9 is more complex. If the cw-ESR spectra match the wavelets, the denoising can be extremely effective. Thus, we used coiflet 3 as the wavelet because it best resembles the spectra. Other coiflets and wavelets such as daubechies and symlet did not perform as well as coiflet 3.

The new method is compared with the standard SUREShrink and Minimax methods [29], [31] using both hard and soft thresholding as well as other wavelet

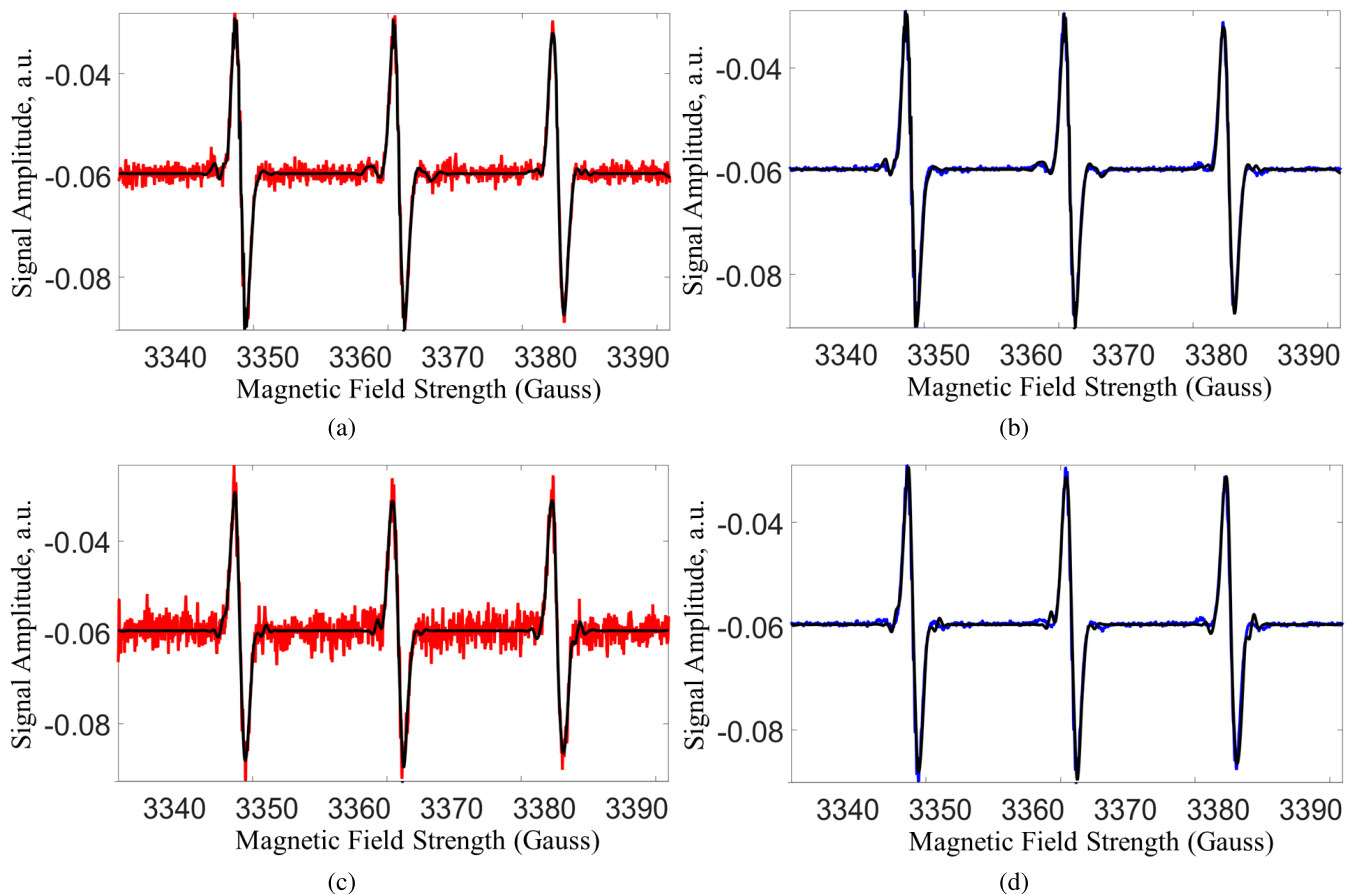


**FIGURE 4.** Example 1: New Method Denoising results at 16 and 4 scans, respectively. The cw-ESR spectrum was obtained from a sample of the nitroxide spin probe *tempol* in a 0.1 mM solution in water [47]. The signal amplitude is in arbitrary units (a.u.) and the abscissa is in Gauss. (a) 16 Scans: New Method vs Noisy. (b) 16 Scans: New Method vs Reference (500 scans). (c) 4 Scans: New Method vs Noisy. (d) 4 Scans: New Method vs Reference (500 scans).

denoising methods. We used the two different examples (Figures 5-8 and Figure 9) to show and compare the denoised results. The SUREShrink and Minimax methods are the optimized hybrid scale dependent threshold selection schemes in the current literature [24], [48], whereas other newer methods [9], [37]–[39] use a thresholding function other than hard and soft in an effort to obtain better denoising. Filtering methods are not compared with the new method because standard wavelet denoising methods perform better than them as shown in ESR [30] and in general [24], [25]. The decomposition level  $k$  that yields maximum SNR compared to other decomposition levels is selected for the standard denoising methods. In the new method,  $T_r = 0.20$  was used for all the examples. We have extensively tested (both experimental and model data sets) this value of  $T_r$  as the criterion for noise thresholding and find it succeeds in virtually all cases.

### C. RESULTS

In example 1 (cf. Figures 3-8), the denoised spectra by the new method at 16 and 4 scans in Figure 4 are shown overlapped with the noisy and reference spectra for comparison

and analysis. As can be seen, the new method successfully recovers the signal peaks and removes the baseline noise. Also, the new method retrieves the small satellite peaks (adjacent to large peaks) that were submerged in noise. Comparing the spectra of 16 and 4 scans, the denoised 16 scan spectrum recovers the satellite peaks more accurately than the 4 scan denoised spectrum, as expected. In Figures 5-8 the new method is compared with the denoised spectra of other denoising methods.

Similarly in example 2 (see Figure 9), the new method effectively removes the baseline noise and is better able to retrieve the peaks compared to other denoising methods. Note that the results of non-soft and non-hard thresholding function methods [9], [37]–[39] were similar for example 2, and hence, only Zhang and Song's method [39] is shown. As can be seen, the current state-of-the-art methods are either not very effective at removing baseline noise and/or they distort the signal peak heights.

Tables 1 and 2 show the SNR of the original noisy and denoised spectra, along with decomposition levels selected for noise thresholding. In example 1, it can be seen that the new method doubles the SNR (in dB) from the noisy spectrum



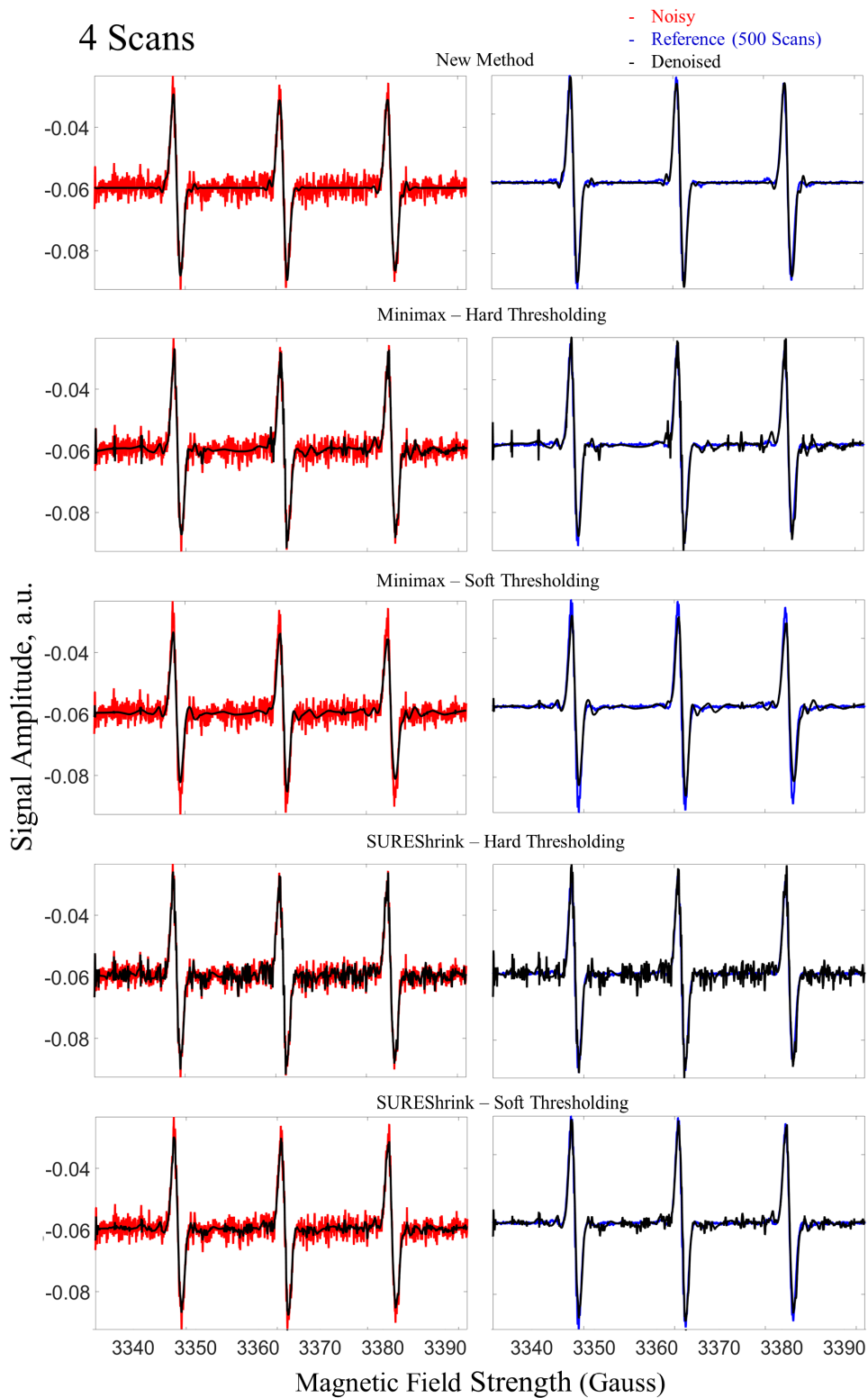


**FIGURE 5.** Experimental Data Example 1: Comparison of New Method with Minimax and SUREShrink Denoising at 4 scans.

and is more than 20 dB greater than other denoising methods. In example 2, which is a more complex but much broader spectrum, the new method increases the SNR by a huge

amount, almost reaching the noiseless state. This is likely due to the low frequency nature of the spectrum versus the higher frequency noise.

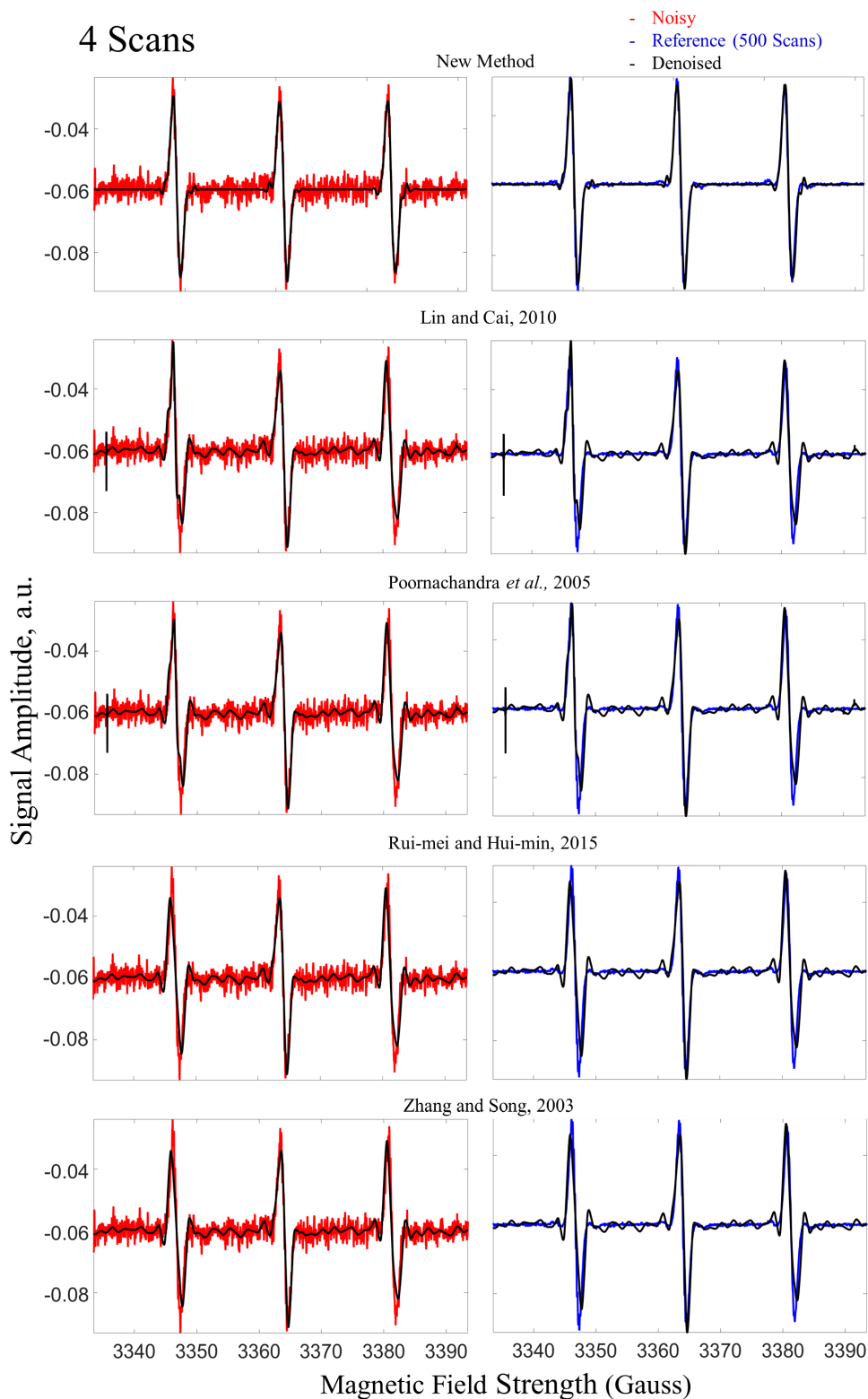


**FIGURE 6.** Example 1: Comparison of New Method with Denoising methods [9], [37]–[39] other than soft and hard thresholding at 4 scans.

For example 1, since there is a good reference signal, the SSIM is also calculated and shown in Table 1. It can be seen that the noisy signal at 16 scans

is structurally very similar to the reference signal, revealing that the noise hardly distorts the signal. But the 4 scan noise possesses some structural distortion. For 16 scans,

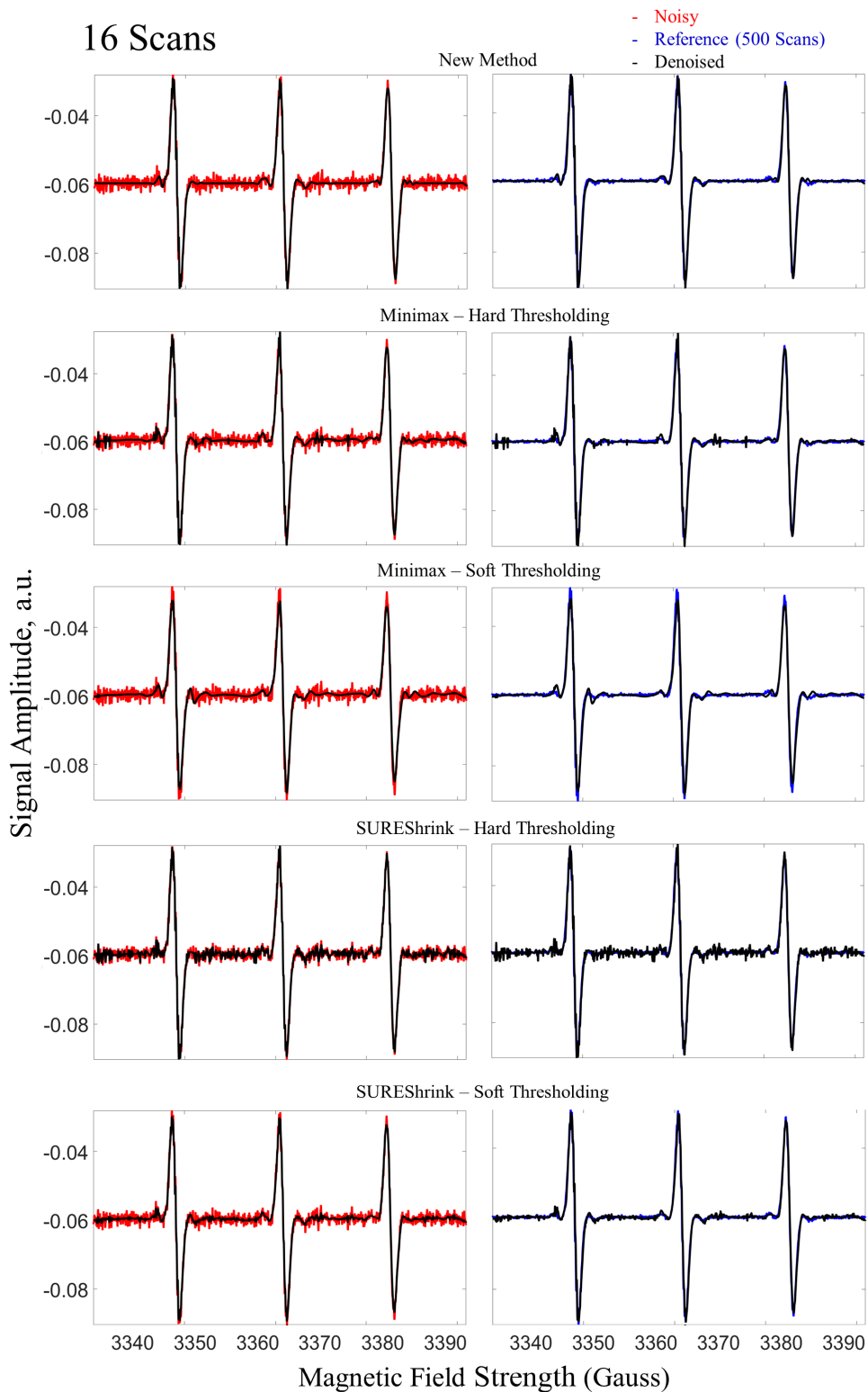
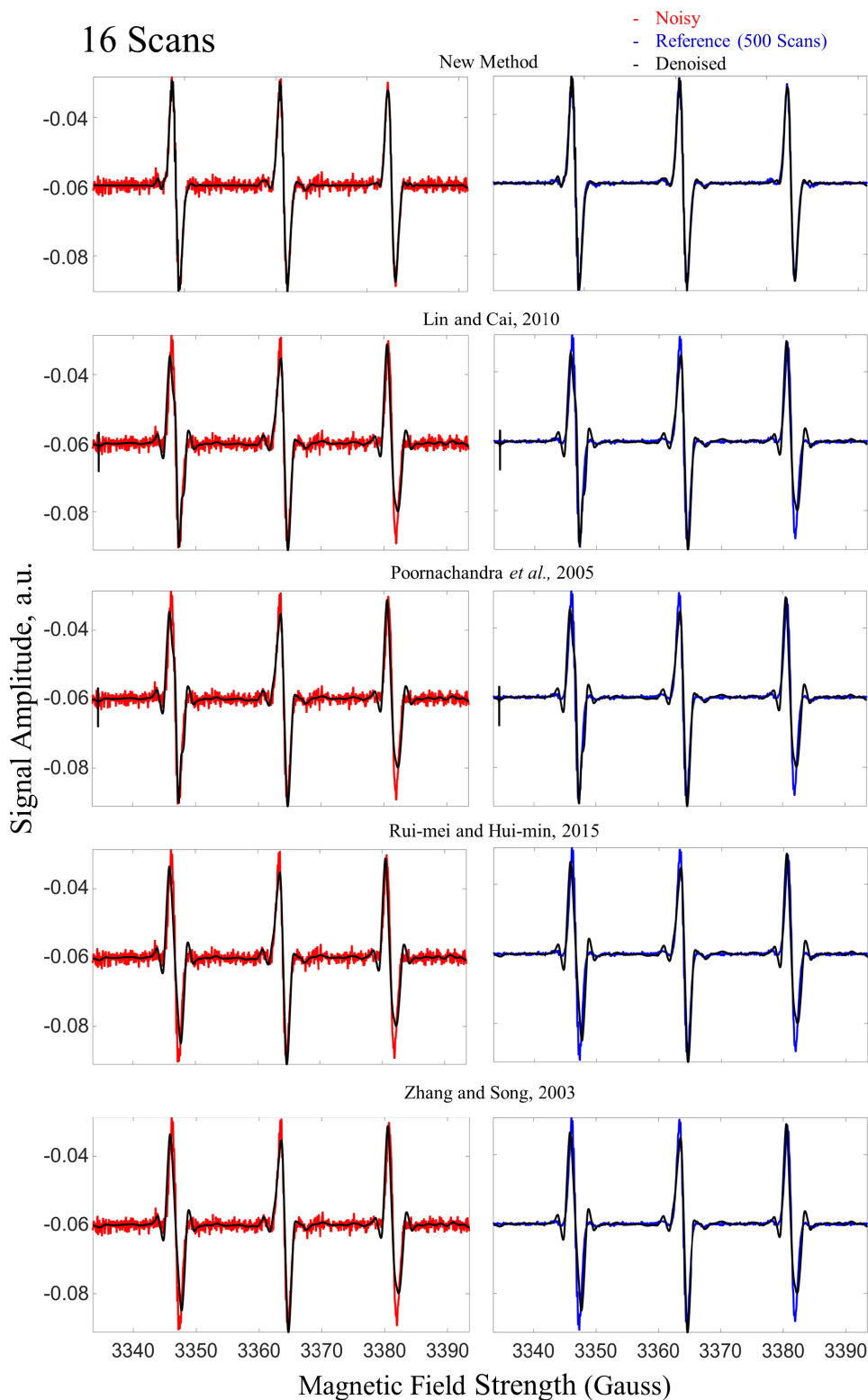


FIGURE 7. Example 1: Comparison of New Method with Minimax and SUREShrink Denoising at 16 scans.

the new method along with SUREShrink and Minimax soft and hard thresholding methods increases the SSIM, while the other methods decrease it. The increase

is highest for the new method. For 4 scans, the new method significantly increases the SSIM, while other denoising methods slightly improve it. At both



**FIGURE 8.** Example 1: Comparison of New Method with Denoising methods [9], [37]–[39] other than soft and hard thresholding at 16 scans.

16 and 4 scans, the new method not only regains the referencesignal maximally but it also resembles it very closely.

Both qualitatively and quantitatively, the new method outperforms the current denoising methods and successfully recovers the desired spectrum.

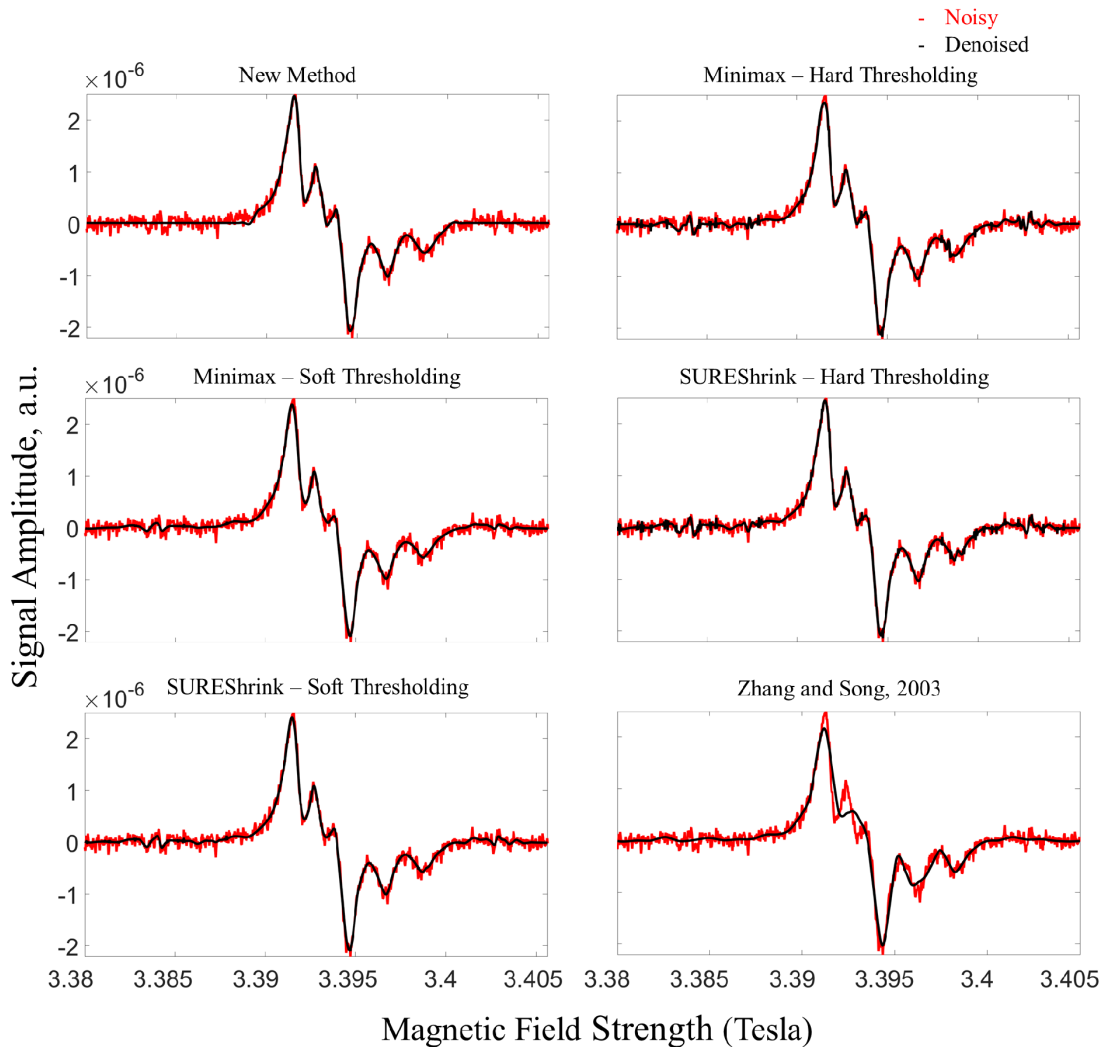


**FIGURE 9.** Example 2: Comparison of New Method with other standard denoising methods. The cw-ESR spectrum was obtained from a sample of a nitroxide-labeled lipid in lipid vesicles.

**TABLE 1.** Example 1 - Signal to Noise Ratio (SNR): Comparison of New Method with other standard wavelet denoising methods at 16 and 4 scans. Hard and Soft represent hard and soft thresholding, respectively; dB is SNR in decibels; and DL is Decomposition Level (cf. Figures 3-8).

Method	16 scans				4 scans			
	SNR (dB)	SNR	SSIM	DL	SNR (dB)	SNR	SSIM	DL
Noisy	35	57	0.9903	-	30	32	0.9684	-
Minimax-Hard	43	146	0.9959	7	38	81	0.9880	7
Minimax-Soft	46	201	0.9954	7	41	114	0.9890	12
SUREShrink-Hard	38	82	0.9938	9	32	41	0.9779	9
SUREShrink-Soft	44	157	0.9966	7	37	77	0.9905	12
Zhao [9]	46	209	0.9821	6	38	80	0.9790	6
Poornachandra [38]	44	167	0.9825	6	37	73	0.9803	6
Zhang [39]	46	209	0.9821	6	38	80	0.9778	6
Lin [37]	44	167	0.9825	6	38	79	0.9800	6
<b>New Method</b>	<b>73</b>	<b>4438</b>	<b>0.9969</b>	<b>6</b>	<b>64</b>	<b>1567</b>	<b>0.9957</b>	<b>6</b>

**D. COMPUTATIONAL COMPLEXITY**

For the new method as well as the other methods, the computational complexity of DWT, IDWT, plus application of the thresholding function is  $\mathcal{O}(N)$ . However, the new method takes  $\mathcal{O}(N)$  operations to calculate thresholds, as it requires only simple arithmetic operations for

calculating mean, standard deviation, and ratios. On the other hand, the thresholds obtained from SURE and Minimax optimization can take  $\mathcal{O}(N \log N)$  operations. Therefore, overall the new method has computational complexity ( $\mathcal{O}(N)$ ) which is less than the other denoising methods ( $\mathcal{O}(N \log N)$ ).

**TABLE 2. Example 2 - Signal to Noise Ratio (SNR): Comparison of New Method with other standard wavelet denoising methods. dB is SNR in decibels; and DL is Decomposition Level (cf. Figure 9).**

Method	SNR (dB)	SNR	DL
Noisy	33	49	-
Minimax-Hard	38	81	10
Minimax-Soft	43	149	6
SUREShrink-Hard	37	76	7
SUREShrink-Soft	41	115	9
Zhang [39]	44	167	6
<b>New Method</b>	<b>165</b>	<b><math>191 \times 10^6</math></b>	<b>4</b>

**TABLE 3. Example 1 - Computation Time: Comparison of New Method with other standard wavelet denoising methods.**

Method	Computation Time (seconds)	
	16 scans	4 scans
Minimax-Hard	0.0804	0.0834
Minimax-Soft	0.0807	0.0788
SUREShrink-Hard	0.0853	0.0878
SUREShrink-Soft	0.0873	0.0866
Zhao [9]	0.0864	0.0864
Poornachandra [38]	0.0857	0.0849
Zhang [39]	0.0858	0.0855
Lin [37]	0.0867	0.0852
<b>New Method</b>	<b>0.0131</b>	<b>0.0140</b>

Table 3 shows the actual computation times of the new method and other denoising methods for example 1. The computation time was calculated in MATLAB on a 64-bit operating system with 16 GB RAM and a 3.30 GHz processor. To overcome any processing variation in the computer, the computation time was measured 5000 times and then averaged. It can be seen that the new method is more than 6 times faster than other denoising methods.

## VII. CONCLUSIONS

This paper presents a comprehensive framework for wavelet transform denoising illustrating it with denoising of cw-ESR spectra, and it shows the limitations of current wavelet denoising methods. The two examples were chosen as illustrative from over 100 examples of model and experimental data. This new denoising method enables the selection of appropriate thresholds for noise removal. It is shown that this new method is able to effectively denoise and especially retrieve the signal peaks accurately.

There are two advantages of the proposed method. First, it allows the analysis of a low SNR signal by effectively retrieving the relevant information. This is especially beneficial where signals are obtained at low SNR. Second, the new method can be used to minimize the number of scans needed for signal averaging, resulting in large savings in experimental time. In the application of the new method to extensive cw-ESR spectra, we found it to be consistently successful in accurately retrieving the original signal. Theoretically, very extensive signal averaging would remove all the random noise, but due to time constraints, the number of scans that are practical is often limited.

We believe that our new denoising method can be applied to other spectroscopies such as nuclear magnetic

resonance (NMR) spectroscopy [49], Infrared spectroscopy [49], Ultraviolet spectroscopy [49], Raman spectroscopy [50], mass spectroscopy [49], and others that yield 1D spectra. We currently are developing this approach for time domain signals as well as for two- and higher-dimensional spectroscopies.

## ACKNOWLEDGMENT

The authors would like to thank Boris Dzikovski for generating the ESR spectra and useful discussions. This work is covered by U.S. Patent Application No. 62/334,626.

## REFERENCES

- [1] T. Cai and B. W. Silverman, "Incorporating information on neighbouring coefficients into wavelet estimation," *Sankhyā, Indian J. Statist. B*, vol. 63, no. 2, pp. 127–148, 2001.
- [2] J. Jiang, J. Guo, W. Fan, and Q. Chen, "An improved adaptive wavelet denoising method based on neighboring coefficients," in *Proc. 8th World Congr. Intell. Control Autom.*, Jul. 2010, pp. 2894–2898.
- [3] G. Y. Chen and T. D. Bui, "Multiwavelets denoising using neighboring coefficients," *IEEE Signal Process. Lett.*, vol. 10, no. 7, pp. 211–214, Jul. 2003.
- [4] G. Y. Chen, T. D. Bui, and A. Krzyzak, "Image denoising using neighbouring wavelet coefficients," *Integr. Comput.-Aided Eng.*, vol. 12, no. 1, pp. 99–107, 2005.
- [5] D. Zhou and W. Cheng, "Image denoising with an optimal threshold and neighbouring window," *Pattern Recognit. Lett.*, vol. 29, no. 11, pp. 1694–1697, 2008.
- [6] S. Madhu, H. B. Bhavani, S. Sumathi, and H. A. Vidya, "A novel algorithm for denoising of simulated partial discharge signals using adaptive wavelet thresholding methods," in *Proc. 2nd Int. Conf. Electron. Commun. Syst. (ICECS)*, Feb. 2015, pp. 1596–1602.
- [7] R. Hussein, K. B. Shaban, and A. H. El-Hag, "Histogram-based thresholding in discrete wavelet transform for partial discharge signal denoising," in *Proc. Int. Conf. Commun., Signal Process., Appl. (ICCSPA)*, 2015, pp. 1–5.
- [8] A. E. Cetin and M. Tofghi, "Projection-based wavelet denoising [lecture notes]," *IEEE Signal Process. Mag.*, vol. 32, no. 5, pp. 120–124, Sep. 2015.
- [9] R.-M. Zhao and H.-M. Cui, "Improved threshold denoising method based on wavelet transform," in *Proc. 7th Int. Conf. Modelling, Identificat. Control (ICMIC)*, 2015, pp. 1–4.
- [10] Y. Ding and I. W. Selesnick, "Artifact-free wavelet denoising: Non-convex sparse regularization, convex optimization," *IEEE Signal Process. Lett.*, vol. 22, no. 9, pp. 1364–1368, Sep. 2015.
- [11] Q. Zhao and W. Dai, "A wavelet denoising method of new adjustable threshold," in *Proc. IEEE 16th Int. Conf. Commun. Technol. (ICCT)*, Oct. 2015, pp. 684–688.
- [12] Z. Madadi, G. V. Anand, and A. B. Premkumar, "Signal detection in generalized Gaussian noise by nonlinear wavelet denoising," *IEEE Trans. Circuits Syst. I, Reg. Papers*, vol. 60, no. 11, pp. 2973–2986, Nov. 2013.
- [13] G. Deng and Z. Liu, "A wavelet image denoising based on the new threshold function," in *Proc. 11th Int. Conf. Comput. Intell. Secur. (CIS)*, Dec. 2015, pp. 158–161.
- [14] V. C. Bibina and S. Viswasom, "Adaptive wavelet thresholding & joint bilateral filtering for image denoising," in *Proc. Annu. IEEE India Conf. (INDICON)*, Dec. 2012, pp. 1100–1104.
- [15] S. Guo, F. Wu, W. Wei, J. Guo, Y. Ji, and Y. Wang, "A novel wavelet denoising method used for droplet volume detection in the microfluidic system," in *Proc. IEEE Int. Conf. Mechatronics Autom.*, Aug. 2013, pp. 1732–1737.
- [16] G. Chen, W. Xie, and Y. Zhao, "Wavelet-based denoising: A brief review," in *Proc. 4th Int. Conf. Intell. Control Inf. Process. (ICICIP)*, 2013, pp. 570–574.
- [17] S. G. Chang, B. Yu, and M. Vetterli, "Spatially adaptive wavelet thresholding with context modeling for image denoising," *IEEE Trans. Image Process.*, vol. 9, no. 9, pp. 1522–1531, Sep. 2000.
- [18] L. Sendur and I. W. Selesnick, "Bivariate shrinkage functions for wavelet-based denoising exploiting interscale dependency," *IEEE Trans. Signal Process.*, vol. 50, no. 11, pp. 2744–2756, Nov. 2002.
- [19] A. Pizurica and W. Philips, "Estimating the probability of the presence of a signal of interest in multiresolution single- and multiband image denoising," *IEEE Trans. Image Process.*, vol. 15, no. 3, pp. 654–665, Mar. 2006.

- [20] M. Jansen and A. Bulthel, "Empirical Bayes approach to improve wavelet thresholding for image noise reduction," *J. Amer. Statist. Assoc.*, vol. 96, no. 454, pp. 629–639, Jun. 2001.
- [21] Y. Liu and X. Cheng, "A new signal denoising algorithm from wavelet modulus maxima," in *Proc. 4th Int. Conf. Fuzzy Syst. Knowl. Discovery*, Aug. 2007, pp. 32–35.
- [22] S. G. Mallat, "A theory for multiresolution signal decomposition: The wavelet representation," *IEEE Trans. Pattern Anal. Mach. Intell.*, vol. 11, no. 7, pp. 674–693, Jul. 1989.
- [23] X. Meng, Z. He, G. Feng, and B. Xiao, "An improved wavelet denoising algorithm for wideband radar targets detection," *Circuits Syst. Signal Process.*, vol. 32, no. 4, pp. 2003–2026, 2013.
- [24] I. K. Fodor and C. Kamath, "Denoising through wavelet shrinkage: An empirical study," *J. Electron. Imag.*, vol. 12, no. 1, pp. 1200–1224, 2003.
- [25] A.-M. Wink and J. B. T. M. Roerdink, "Denoising functional MR images: A comparison of wavelet denoising and Gaussian smoothing," *IEEE Trans. Med. Imag.*, vol. 23, no. 3, pp. 374–387, Mar. 2004.
- [26] R. R. Ernst, "Sensitivity enhancement in magnetic resonance. I. Analysis of the method of time averaging," *Rev. Sci. Instrum.*, vol. 36, no. 12, pp. 1689–1695, 1965.
- [27] J. A. Weil and J. R. Bolton, *Electron Paramagnetic Resonance: Elementary Theory and Practical Applications*. New York, NY, USA: Wiley, 1994.
- [28] A. C. Kak and M. Slaney, *Principles of Computerized Tomographic Imaging*. New York, NY, USA: IEEE Press, 1988.
- [29] D. L. Donoho, "De-noising by soft-thresholding," *IEEE Trans. Inf. Theory*, vol. 41, no. 3, pp. 613–627, May 1995.
- [30] J. H. Bryant, "Electron paramagnetic resonance image reconstruction for arbitrary projection sampling and regions of interest," Ph.D. dissertation, Dept. Med. Imag. Radiol., Oncology, Univ. Chicago, Chicago, IL, USA, 2011.
- [31] D. L. Donoho and I. M. Johnstone, "Ideal spatial adaptation via wavelet shrinkage," *Biometrika*, vol. 81, no. 3, pp. 425–455, 1994.
- [32] I. M. Johnstone and B. W. Silverman, "Wavelet threshold estimators for data with correlated noise," *J. Roy. Statist. Soc.*, vol. 59, no. 2, pp. 319–351, 1997.
- [33] F. Chang, W. Hong, T. Zhang, J. Jing, and X. Liu, "Research on wavelet denoising for pulse signal based on improved wavelet thresholding," in *Proc. 1st Int. Conf. Pervas. Comput. Signal Process. Appl. (PCSPA)*, Sep. 2010, pp. 564–567.
- [34] C. M. Stein, "Estimation of the mean of a multivariate normal distribution," *Ann. Statist.*, vol. 9, no. 6, pp. 1135–1151, 1981.
- [35] D. L. Donoho and I. M. Johnstone, "Adapting to unknown smoothness via wavelet shrinkage," *J. Amer. Statist. Assoc.*, vol. 90, no. 432, pp. 1200–1224, 1995.
- [36] H.-Y. Gao, "Wavelet shrinkage denoising using the non-negative garrote," *J. Comput. Graph. Statist.*, vol. 7, no. 4, pp. 469–488, 1998.
- [37] Y. Lin and J. Cai, "A new threshold function for signal denoising based on wavelet transform," in *Proc. IEEE Int. Conf. Meas. Technol. Mechatronics Autom.*, Mar. 2010, pp. 200–203.
- [38] S. Poornachandra, N. Kumaravel, T. K. Saravanan, and R. Somaskandan, "WaveShrink using modified hyper-shrinkage function," in *Proc. 27th Annu. Int. Conf. Eng. Med. Biol. Soc. (IEEE-EMBS)*, Jan. 2005, pp. 30–32.
- [39] D. Zhang and P. Bao, "Denoising by spatial correlation thresholding," *IEEE Trans. Circuits Syst. Video Technol.*, vol. 13, no. 6, pp. 535–538, Jun. 2003.
- [40] J. Freed, "New technologies in electron spin resonance," *Annu. Rev. Phys. Chem.*, vol. 51, no. 1, pp. 655–689, 2000.
- [41] J. H. Freed, "ESR and molecular dynamics," in *Biomedical EPR, Part B: Methodology, Instrumentation, and Dynamics*. Boston, MA, USA: Springer, 2005, pp. 239–268.
- [42] Z. Zhang et al., "Multifrequency electron spin resonance study of the dynamics of spin labeled T4 lysozyme," *J. Phys. Chem. B*, vol. 114, no. 16, pp. 5503–5521, 2010.
- [43] W. Hofbauer, K. A. Earle, C. R. Dunnam, J. K. Moscicki, and J. H. Freed, "High-power 95 GHz pulsed electron spin resonance spectrometer," *Rev. Sci. Instrum.*, vol. 75, no. 5, pp. 1194–1208, 2004.
- [44] C. Poole, *Electron Spin Resonance: A Comprehensive Treatise on Experimental Techniques*. New York, NY, USA: Courier Corporation, 1996.
- [45] K. A. Earle, B. Dzikovski, W. Hofbauer, J. K. Moscicki, and J. H. Freed, "High-frequency ESR at ACERT," *Magn. Reson. Chem.*, vol. 43, no. S1, pp. S256–S266, 2005.
- [46] Z. Wang, A. C. Bovik, H. R. Sheikh, and E. P. Simoncelli, "Image quality assessment: From error visibility to structural similarity," *IEEE Trans. Image Process.*, vol. 13, no. 4, pp. 600–612, Apr. 2004.
- [47] B. G. Dzikovski and V. A. Livshits, "EPR spin probe study of molecular ordering and dynamics in monolayers at oil/water interfaces," *Phys. Chem. Chem. Phys.*, vol. 5, pp. 5271–5278, Oct. 2003.
- [48] R. Cohen, "Signal denoising using wavelets," Dept. Elect. Eng., Technion-Israel Inst. Technol., Haifa, Israel, Tech. Rep., 2012.
- [49] D. Pavia, G. Lampman, G. Kriz, and J. Vyvyan, *Introduction to Spectroscopy*. Boston, MA, USA: Cengage Learning, 2008.
- [50] C. M. Galloway, E. C. Le Ru, and P. G. Etchegoin, "An iterative algorithm for background removal in spectroscopy by wavelet transforms," *Appl. Spectrosc.*, vol. 63, no. 12, pp. 1370–1376, 2009.



**MADHUR SRIVASTAVA** (S'11) received the B.Tech. degree in electronics and communication engineering from the Jaypee University of Engineering and Technology (JUET), Guna, India, in 2011, the M.Eng. degree in electrical and computer engineering and the M.S. degree in biomedical engineering from Cornell University, Ithaca, NY, USA, in 2012. He is currently pursuing the Ph.D. degree with the Meinig School of Biomedical Engineering, and doing research with

the National Biomedical Center for Advanced ESR Technology, Cornell University.

He was involved in summer internship with the Indian Institute of Science Education and Research-Kolkata, Nadia, India, in 2010. From 2012 to 2013, he was a Research Staff Member with the Department of Biological and Environmental Engineering and also a Research Assistant of the Speech Imaging Group with Cornell University. In 2015, he was involved in a summer immersion program with Weill Cornell Medical College, New York, NY, USA. His research interests include signal and image processing, magnetic resonance, and quantum computing.

Mr. Srivastava is also a Student Member of the International Electron Paramagnetic Resonance Society, the New York Academy of Sciences, and the Institution of Electronics and Telecommunications Engineers (IETE). He served as a Treasurer of the IETE Student Forum of JUET Chapter from 2009 to 2010. He was a recipient of the Vice-Chancellor's Gold Medal at JUET (2011) and the Ph.D. Commercialization Fellowship at Cornell University (2016).



**C. LINDSAY ANDERSON** (M'01) received the B.Sc. (Eng.) and M.Sc. degrees in environmental engineering from the University of Guelph, Guelph, ON, Canada, and the Ph.D. degree in applied mathematics from the University of Western Ontario, London, ON, Canada, in 2004.

She is currently an Assistant Professor with the Department of Biological and Environmental Engineering and the Norman R. Scott Sesquicentennial Faculty Fellow with Cornell University, Ithaca, NY, USA. She has authored several publications. Her research interests include using a systems approach to renewable energy integration. This is an interdisciplinary research area with aspects of operations, optimization, and environmental and systems engineering.

Prof. Anderson holds field memberships (i.e., supervises graduate students) of Electrical and Computer Engineering and Systems Engineering with Cornell University, and an Adjunct Appointment of Applied Mathematics with Western University. She was a recipient of the National Science Foundation Career Award (2015), the Mr. and Mrs. Richard F. Tucker Teaching Award by Cornell University (2011), the Doctoral Dissertation Award by the Canadian Applied and Industrial Mathematics Society (2004), and the University Faculty Award by the Natural Sciences and Engineering Research Council of Canada (2004).



**JACK H. FREED** received the B.E. degree in chemical engineering from Yale University, New Haven, CT, USA, in 1958, and the M.S. and Ph.D. degrees in chemistry from Columbia University, New York, NY, USA, in 1959 and 1962, respectively.

He was a Post-Doctoral Fellow with the University of Cambridge, Cambridge, U.K. from 1962 to 1963. In 1963, he accepted a Faculty Appointment with Cornell University, Ithaca, NY, USA, where he has spent his subsequent career as an Assistant Professor from 1963 to 1967; an Associate Professor from 1967 to 1973; and a Professor from 1973 to 2016; an Emeritus since 2016; and a Frank and Robert Laughlin Professor of Physical Chemistry since 2007. He has been the Director of the National Biomedical Center for Advanced ESR Technology since 2001. He has also held positions as a Visiting Scientist with the U.S. Japan Cooperative Science Program, Tokyo University, Japan (1969); a Guest Professor with Aarhus University, Denmark (1974), a Visiting Professor with the University of Geneva, Switzerland (1977); a Visiting Professor with the Delft University of Technology, The Netherlands (1978), L'École Normale Supérieure, Paris, France (1984-1985), and the University of Padua, Italy (1991); a Charles A. MacDowell Lecturer of Chemical Physics with University of British Columbia (1997); a Distinguished Visiting Professor with Yamagata University, Japan (1998); a Visiting Scientist with the University of Oxford, U.K. (2007-2013); and a Israel Pollak Distinguished Lecturer with the Technion, Israel (2009). He has authored over 400 publications and holds several patents. His interests include the development of modern technology for electron-spin resonance (ESR) spectroscopy both in the development of modern spectrometers and in the theoretical interpretation of ESR experiments designed to elucidate the structural dynamics of complex fluids, such as liquid crystals and membranes, and the structure/function of membrane proteins and protein complexes.

Prof. Freed is a fellow of the American Physical Society (1976), the American Academy of Arts and Sciences (1994), the Royal Society of Chemistry (2009), and the American Association for the Advancement of Science (2009). He has also been an Honorary U.S. Ramsay Memorial Fellow (1962–1963), an NSF Post-Doctoral Fellow at Cambridge University (1962–1963), an A. P. Sloan Foundation Fellow (1966–1968), the Weizmann Institute of Science Senior Fellow (1970), John Simon Guggenheim Memorial Fellow (1984–1985), the Institute for Advanced Studies, The Hebrew University of Jerusalem (1990), and an Inaugural Fellow of the International Society of Magnetic Resonance (2008). In 2001, he became an Honorary Member of the National Magnetic Resonance Society of India. Since 2006, he has been on the External Advisory Board of the National High Magnetic Field Laboratory, USA. He has served on many journal editorial boards, including the *Journal of Chemical Physics* (1976–1978), the *Journal of Physical Chemistry* (1979–1983), *Chemical Physics Letters* (1988–1990), *Applied Magnetic Resonance* (1990–2016), and *Magnetic Resonance Review* (1994–2000), and was an Associate Editor of the *Journal of Magnetic Resonance* (2007–2010). He chaired the Gordon Research Conference on Magnetic Resonance in 1975. From 2008 to 2010, he was the President of the International EPR/ESR Society. Among his awards are the Buck-Whitney Award in Pure and Applied Chemistry (1981) by the American Chemical Society (ACS); the Bruker Award in ESR by the Royal Society of Chemistry (1990); the International Electron Spin Resonance Society Gold Medal (1994); the Irving Langmuir Prize in Chemical Physics by the American Physical Society (1997); the Zavoisky Prize in ESR by the Russian Academy of Sciences (1998); the E. Bright Wilson Award in Spectroscopy by the ACS (2008); the ISMAR Prize from the International Society of Magnetic Resonance (2013); and the Joel H. Hildebrand Award in the Chemistry of Liquids by the ACS (2014). In honor of his extensive achievements, the *Journal of Physical Chemistry* issued a special J.H. Freed Festschrift Issue in 2004 on his 65th birthday.

...